Supplementary Information

Efficient and selective film separation of organism/salt with graded nanofluid channels stimulated by a rigid crystal skeleton

Tianmeng Zhang, [a] Hao Tan, [a] Yao Du, [a] Haimeng Huang, [a] Mingxia Shen, [a] Xing Liu, [b] Zhongchang Wang, [c] Jianfeng Zhang *[a]

[a] College of Mechanics and Materials, Hohai University, Nanjing 211100, PR China

[b] State Key Laboratory of Solidification Processing, School of Materials Science and Engineering, Northwestern Polytechnical University, Xi'an 710072, China

[c] Department Quantum & Energy Material, International Iberian Nanotechnology Laboratory, Braga 4715-330, Portugal

* Corresponding author, Prof. Dr. Jianfeng Zhang

College of Mechanics and Materials, Hohai University

Xikang Road-1, Gulou District, Nanjing 210098, PR China

Tel/fax: +86-25-83787865, Email: jfzhang_sic@163.com

Materials

Pyrrole (Py), Ferrous chloride tetrahydrate ($FeCl_2 \cdot 4H_2O$, ≥ 99%) and hydrogen peroxide (H_2O_2, 30%) were obtained from Aladdin Chemical Reagent Co., Ltd. (Shanghai, China). Bacterial cellulose (BC) was purchased from Guilin Qihong Technology Co., Ltd. (Guangxi, China). Zinc nitrate hexahydrate ($Zn(NO_3)_2 \cdot 6H_2O$, 98%), 2-methylimidazole (MIM, 99%), 3-amino-1,2,4-triazole (Atz, ≥ 95%), 1,3,5-Benzenetricarboxylic chloride (TMC, > 99%), n-hexane, methanol and ethanol were purchased from Aladdin and Sinopharm Chemical Reagent Co., Ltd and used without further purification. The inorganic salts and dyes involved in the experiments were purchased from Sinopharm Chemical Reagent Co., Ltd. (Shanghai, China).

Synthesis of Polypyrrole Sub-micron Spheres (PMs). Firstly, 0.1 g of $FeCl_2 \cdot 4H_2O$ was dissolved in 60 mL of distilled water, and then 1mL of pre-dispersed pyrrole monomer was added and stirred for 30 min. Then 5 mL of H_2O_2 (30 wt%) was added and stirred at room temperature for 12 h. The precipitate was collected by centrifugation and washed several times with acetone and deionized water. Finally, polypyrrole sub-micron spheres, abbreviated as PMs, were obtained by drying at 60 °C.

Synthesis of ZPMs. The specific conditions are as follows: 0.5 wt% of PPSM and 0.06 M of $Zn(NO_3)_2 \cdot 6H_2O$ were dispersed in 40 mL of aqueous ethanol ($V_{ethanol}$: V_{H2O}=2:5) and stirred at room temperature for 1h, then 40ml of 0.6 M MIM ethanol solution was rapidly poured into the above solution and the reaction was continuously stirred for 4 h. At last, the reaction product was repeatedly washed with ethanol and dried under vacuum at 60 °C for 10 h to obtain solid powder ZIF-8@PMs (ZPMs).

Synthesis of ZNPMs. The post-synthetic modification method was used for the synthesis of ZNPMs. 0.4 g of ZPMs was activated at 150 °C for 5 h, and then was dispersed in 150 mL of methanol by water bath sonication for 30 min. 1 g of Atz powder was added to the above suspension, and the reaction was carried out at 50 °C for 20 h. The final product ZIF8-NH_2@PMs (ZNPMs) was obtained by centrifugal washing with methanol and vacuum drying, which is a similar procedure used for the synthesis of ZPMs.

Synthesis of PBC. PPy was coated on the BC by chemical oxidation polymerization,

which was mentioned in our previous study. 2.1 ml of Py was dispersed in 50 mL of BC dispersion (1.5 mg/mL), and then 50ml of oxidant solution (HCl: 2 M, and 0.84 g of $FeCl_3$⓾H_2O) was added and stirred in an ice bath for 10h. The black product was repeatedly washed with deionized water and finally dispersed in 200mL of aqueous solution (containing sodium dodecyl benzene sulfonate: 1 mg/mL).

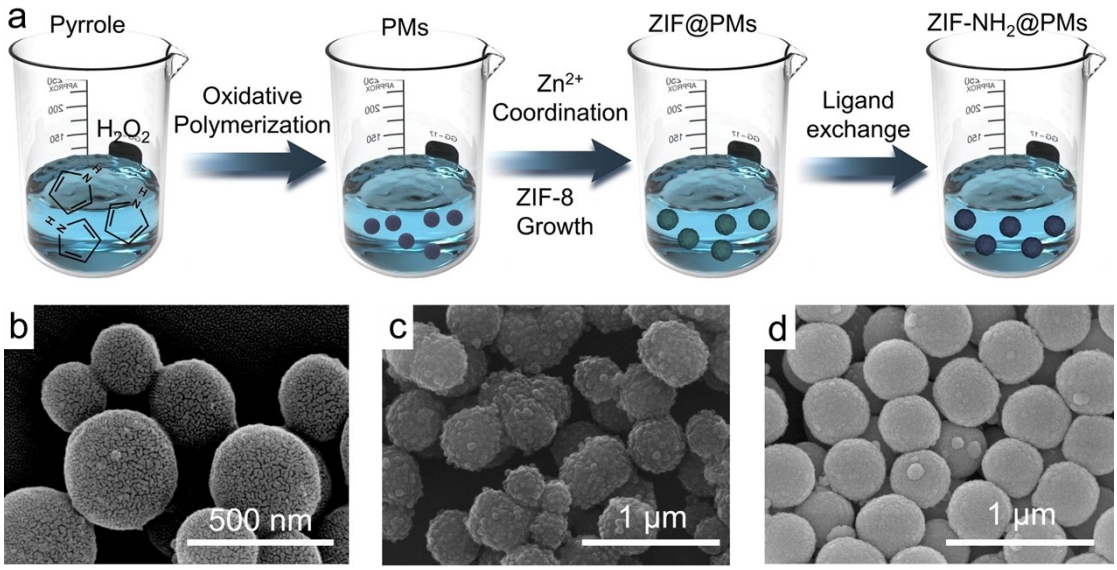

Fig. S1 (a) The preparation process of nano-microspheres; The SEM images of (b) PMs, (c) ZPMs, (d) ZNPMs.

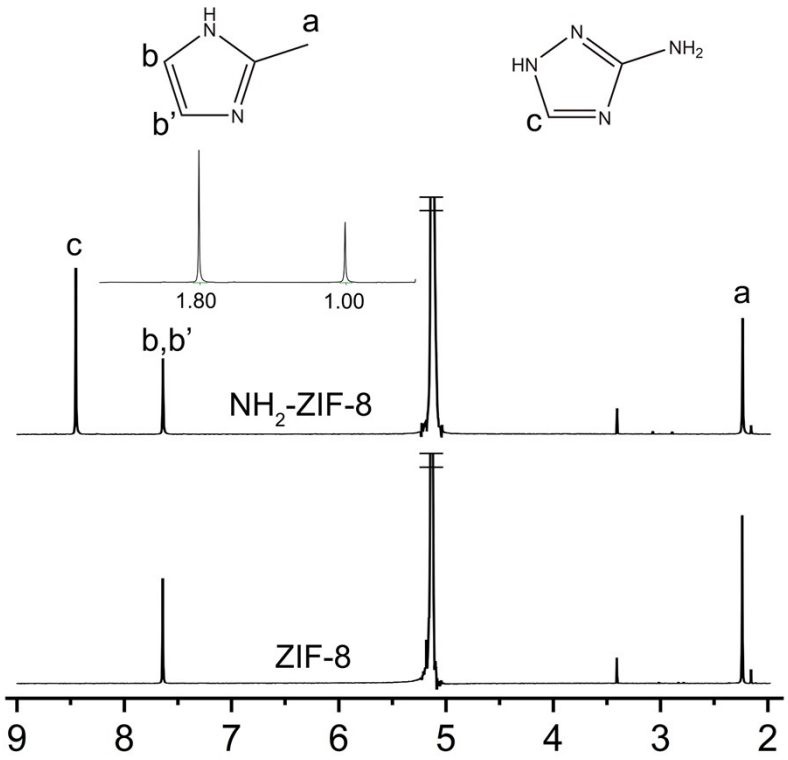

Fig. S2 ^{1}H NMR spectra of ZIF-8 and NH_2-ZIF-8 in the NaOD/D_2O solution.

^{1}H NMR Spectroscopy: Samples were prepared by weighing 2 mg of ZIF into an l.5 mL vial. About 3 to 4 drops of 0.1 M NaOD in the D_2O digestion medium were then added to the vials. This procedure dissolves only the organic portion of the ZIF (linker and modulator); the inorganic component precipitates as zinc oxide or hydroxide. To the mixture, 13 drops of D_2O were added. Then the mixture was centrifuged and the clear supernatant solution was transferred to an NMR tube. ^{1}H NMR spectra were recorded with a Bruker Avance DPX-500 NMR spectrometer (600 MHz; 64 scans). The substitution rate of Atz in ZIF-8 was calculated to be 64% from the test results.

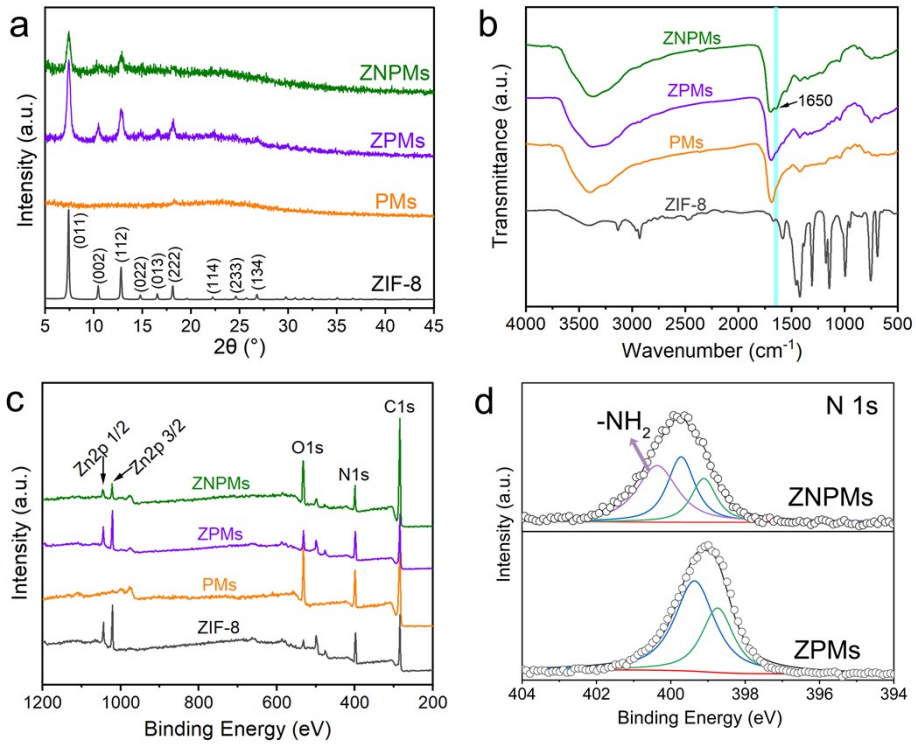

Fig. S3 (a) XRD, (b) FTIR, (c) XPS (d) N1s of nano-particles (ZIF-8, PMs, ZPMs and ZNPMs).

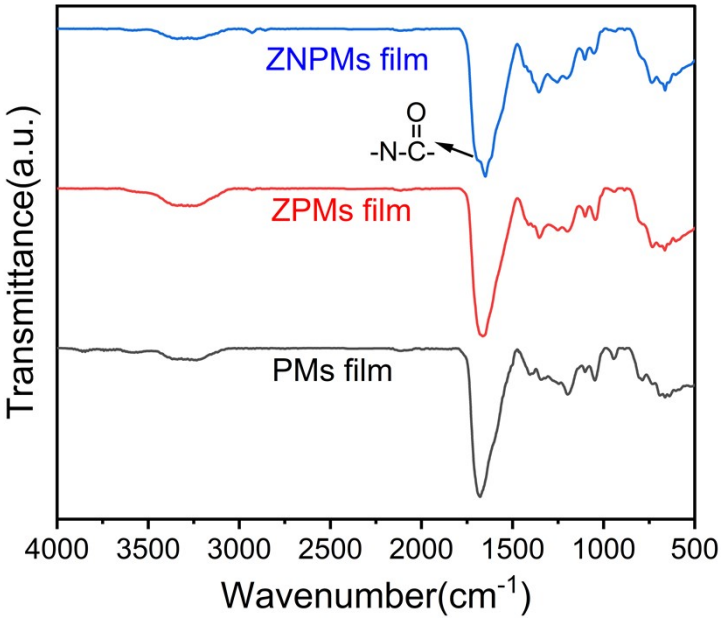

Fig. S4 The FTIR Spectrum of the composite film (PMs, ZPMs and ZNPMs film).

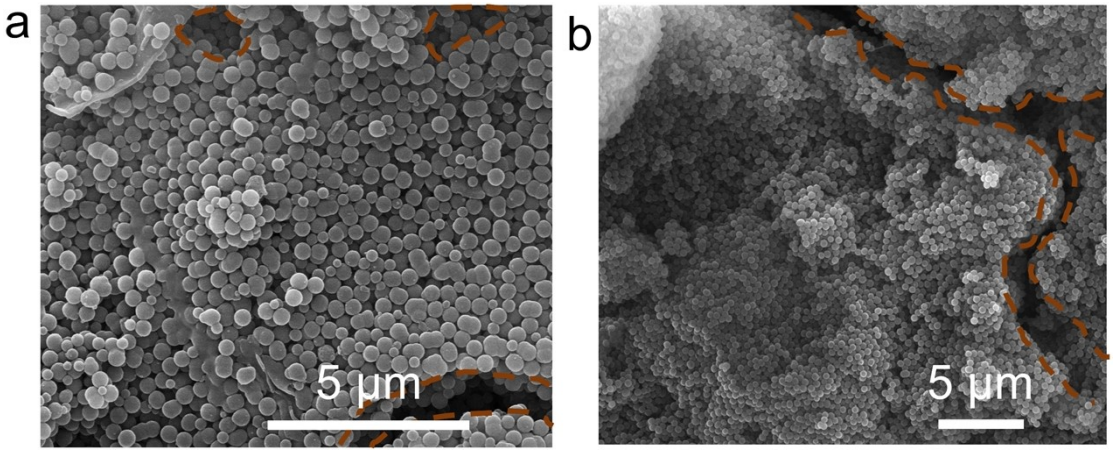

Fig. S5 The surface micromorphology of (a) PMs film and (b)ZPMs film.

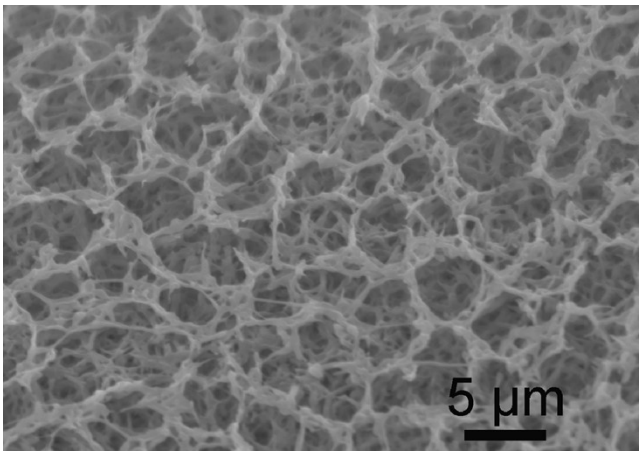

Fig. S6 The SEM image of PVDF substrate film.

The commercial PVDF base film has uniform macropores and is suitable for separating large-scale ions. It cannot separate small-sized solutes such as salts and dyes, and here it is only a substrate film that plays a supporting role.

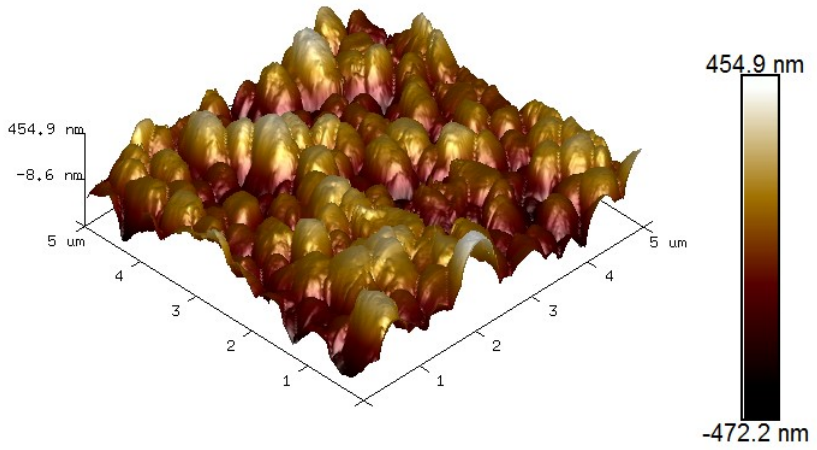

Fig. S7 3D AFM image of ZNPMs film.

The special morphological structure of the film surface is not uncommon. The literature shows that the morphological modulation of micro-nano-level structures on film surfaces is important for special separations, contamination resistance control, and other aspects. Xu et al. prepared MOF nanosheet membranes with honeycomb-like structures and achieved efficient separation of ethanol and water by hydrophobic modification.[1] Li et al. obtained hydrophobic films by interfacial polymerization of self-assembled vesicles of block copolymers, which exhibit a spherical raised structure on the film surface with an order of magnitude increase in permeability during crude oil fractionation.[2] Wang et al. constructed micro-nanoscale regular patterns on the film surface, which can effectively enhance the hydraulic conditions (increase the water flow shear stress and generate local turbulence near the patterns), thus helping to improve the concentration polarization phenomenon and reduce the deposition and adhesion of various contaminants on the film surface.[3] These examples favorably demonstrate that the construction of regular structures on the membrane surface at the micro-nano level can effectively enhance the separation performance.

In this study, the film surface shows the concave and convex structure of the microsphere arrangement, and it is through this arrangement between microspheres that the fluid channel network is constructed, which greatly enhances the water permeability.

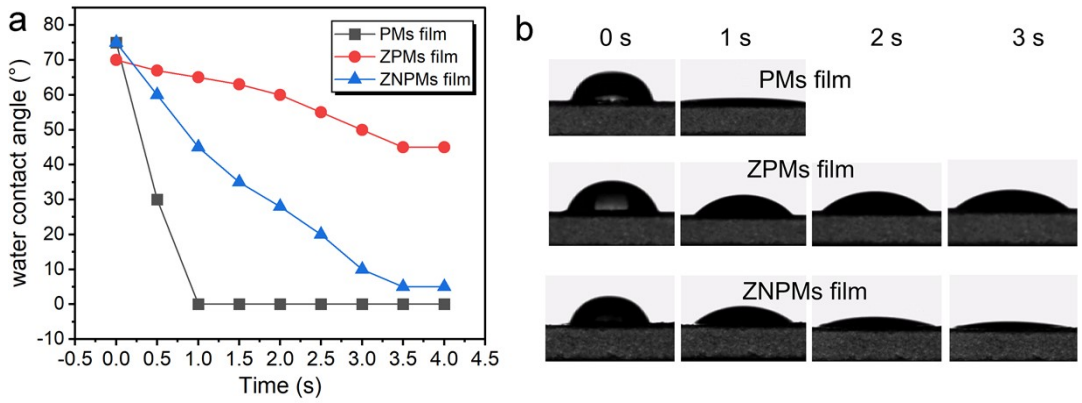

Fig. S8 Water contact angle (a) and digital photos (b) of water adsorbing on PMs, ZPMs and ZNPMs film with time.

The strength of hydrophilicity of the film surface is influenced by the roughness of the film surface and hydrophilic functional groups. PMs films are highly hydrophilic due to the hydrophilic polypyrrole and the carboxyl group of the residual chloride group hydrolyzed in TMC. The film surface of ZNPMs is more hydrophilic than the pristine ZPMs due to the introduction of amino groups.

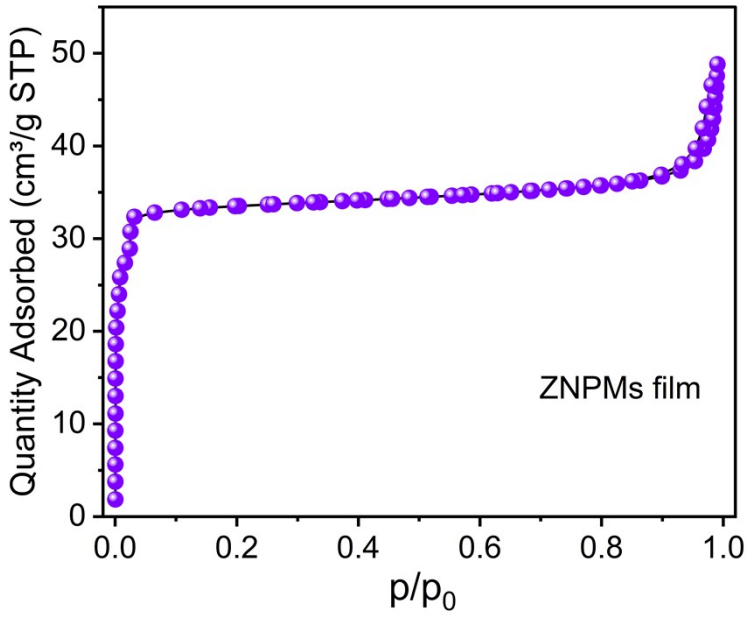

Fig. S9 N_2 adsorption-desorption isotherms of ZNPMs film.

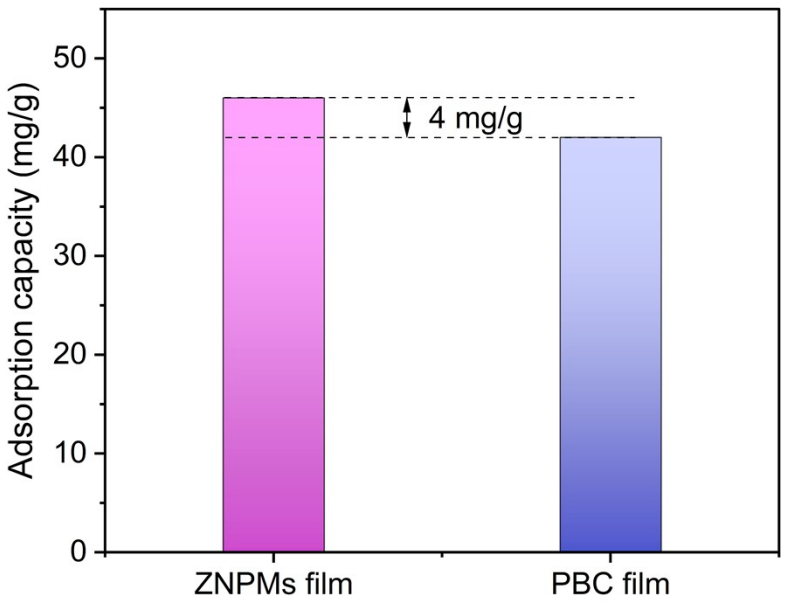

Fig. S10 Adsorption capacity of ZNPMs and PBC films on RhB

The ZNPMs and PBC films were placed in rhodamine B solution and oscillated in a water bath at 25 °C for 24 h to saturate the adsorption. From the adsorption results, it can be seen that the adsorption amount of ZNPMs membrane is only 46 mg/g, which also includes the adsorption amount of PBC layer (42 mg/g). Therefore, the adsorption of the functional layer consisting of microspheres is negligible. Therefore, ZNPMs film is a separation film, not an adsorption film

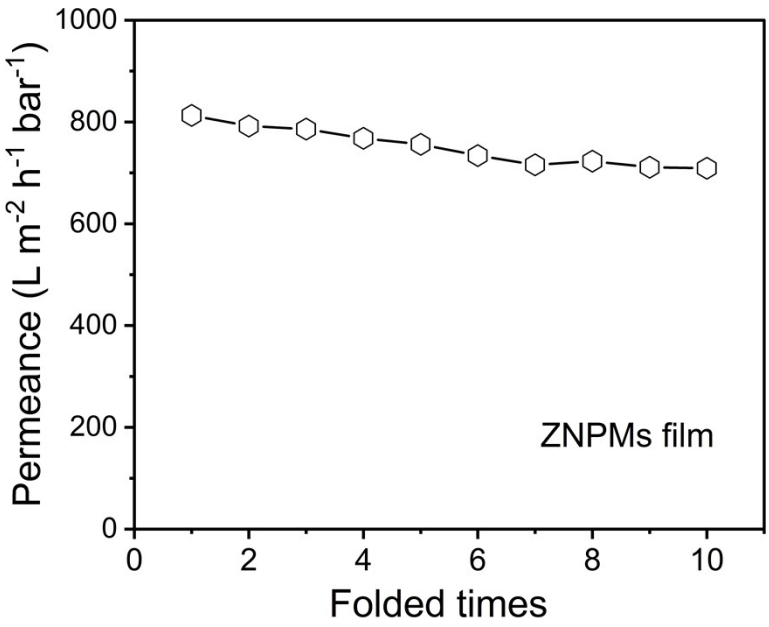

Fig. S11 The change of water permeability of the ZNPMs film after multiple folding

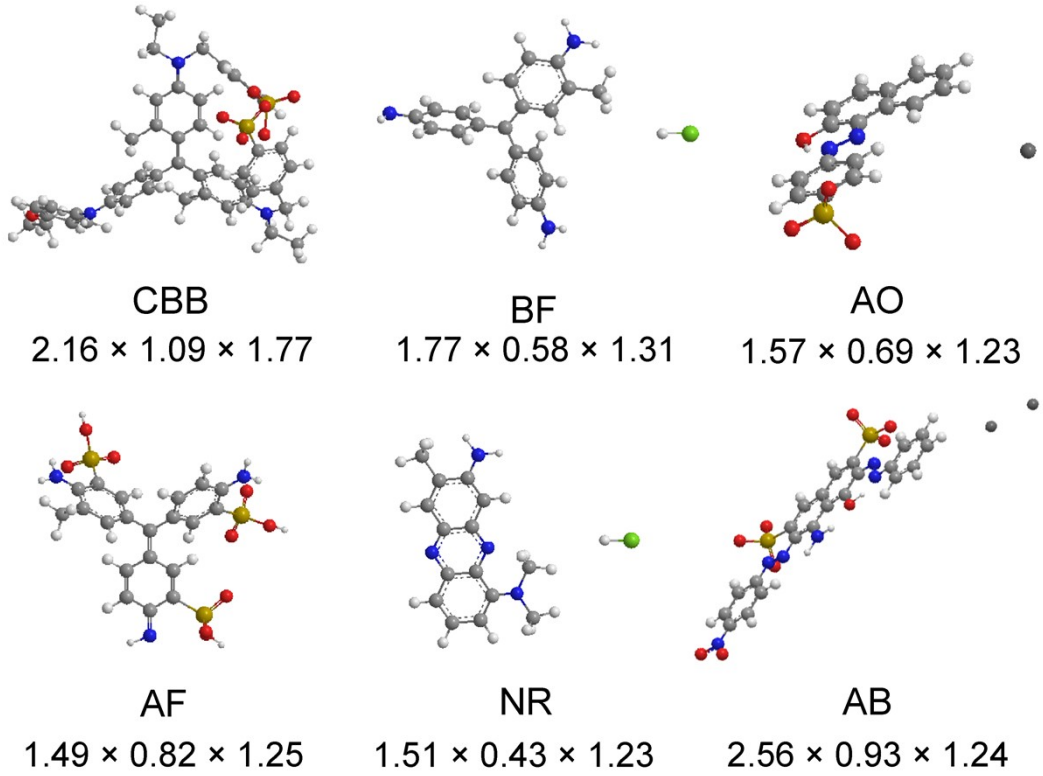

Fig. S12 The molecular structure, and three-dimensional dimensions of the dye molecules (CBB, BF, AO, AF, NR and AB).

From the molecular scale of dyes, the molecular weight ranges from 300 to 800. The selection of different size dyes facilitates the exploration of the film's ability to separate molecules of different sizes. In addition, we selected dyes to cover as many different electrical properties as possible, and includes cationic dyestuffs (e.g., Rhodamine B), anionic dyestuffs (e.g., Amido black 10B) and neutral dyestuffs (e.g., Neutral red). The exploration of the separation behavior of different types of dyes provides a more complete understanding of the properties of composite films.

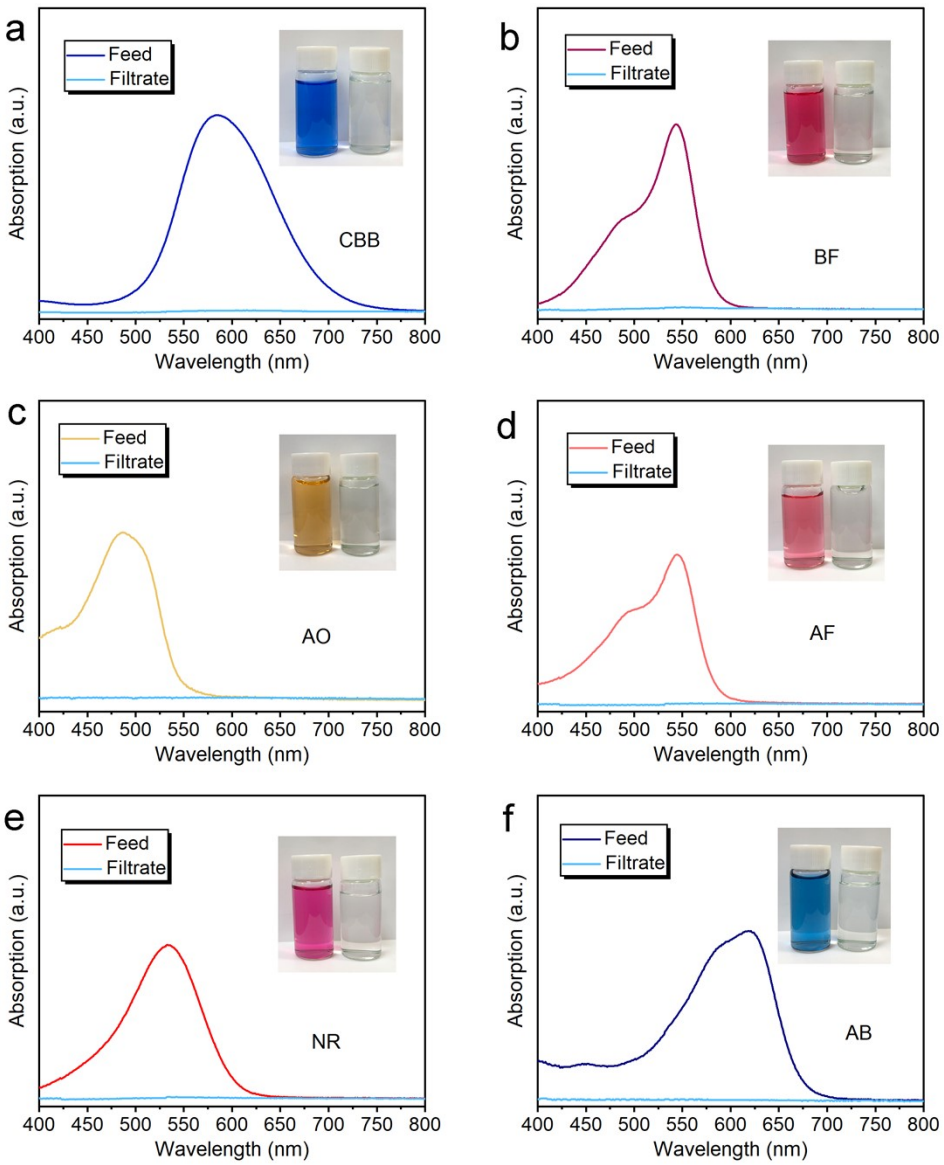

Fig. S13 The UV-Vis absorption spectra and corresponding photographs of CBB, BF, AO, AF, NR and AB solutions before and after separation using the ZNPMs film.

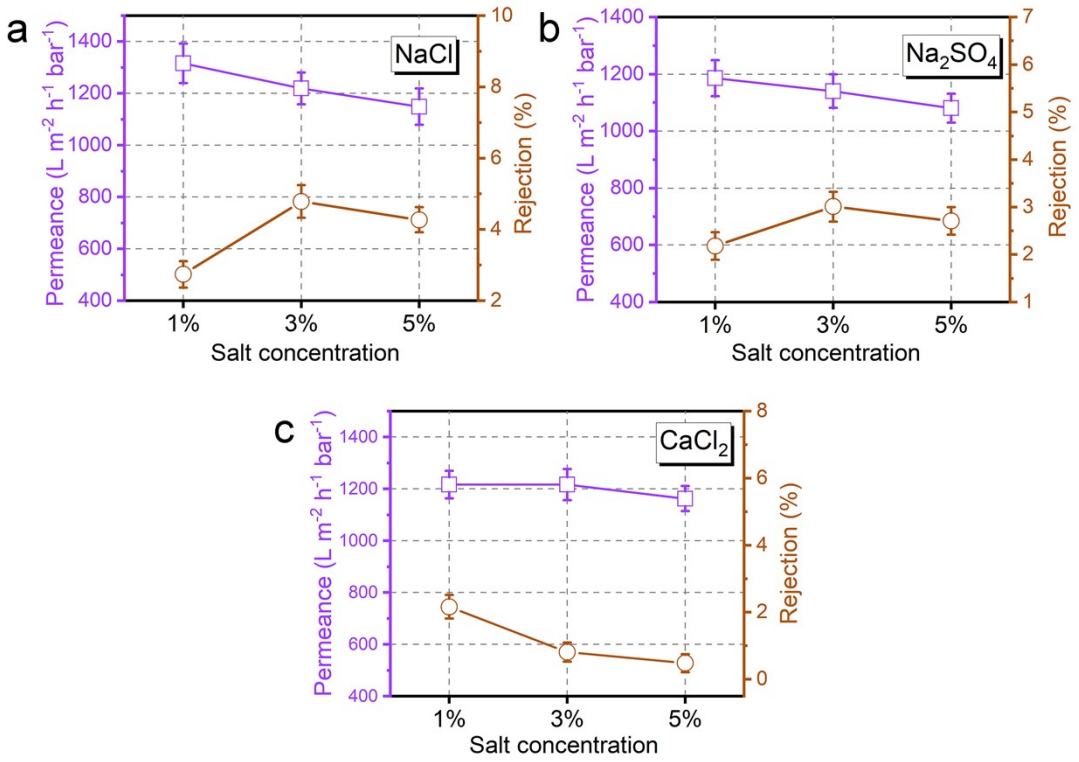

Fig. S14 The separation efficiency of ZNPMs film for different concentrations (1%, 3%, 5%) of salt (a: NaCl; b: Na_2SO_4; c: $CaCl_2$).

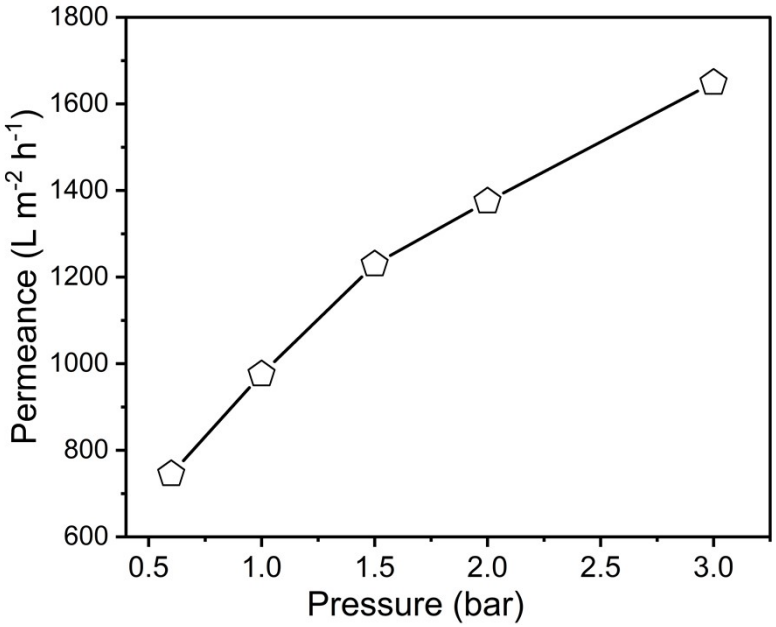

Fig. S15 The water permeance of ZNPMs film at different influent pressures.

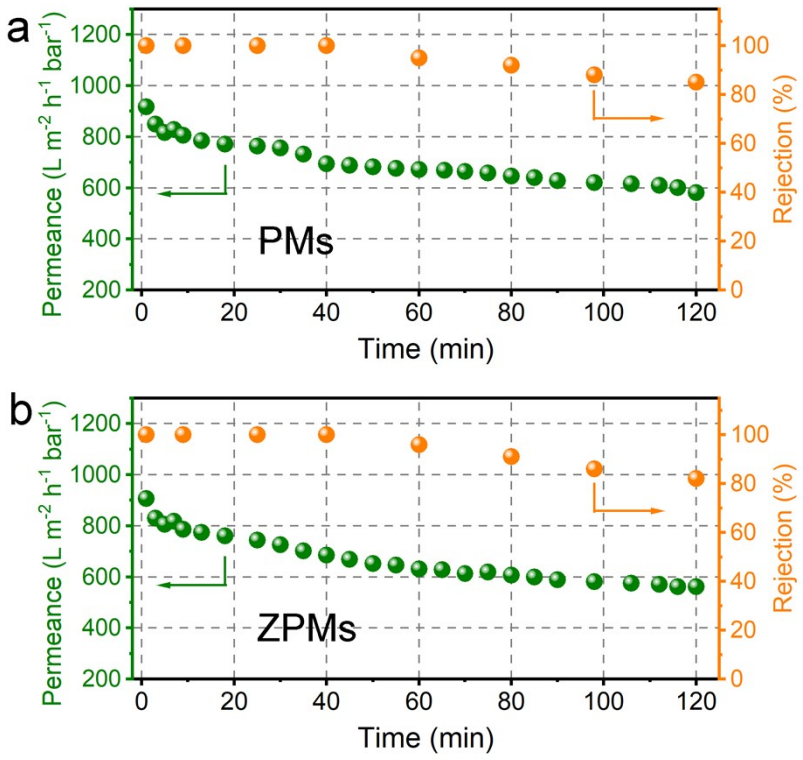

Fig. S16 Water permeability and RhB rejection rate of PMs and ZPMs film under cross-flow filtration (RhB concentration: 5 mg/L).

PMs and ZPMs films exhibit performance in separating dyes at the beginning due to the adsorption of the PBC layer. When the adsorption is saturated, the dye penetrates the film resulting in a decrease in rejection. In PMs and ZPMs films, the weak binding between microspheres leads to the generation of defects on the film surface, resulting in unstable performance. Although they have high flux, the rejection of dyes decreases continuously and cannot meet with the effective separation of dyes/salts.

The more uniform and complete surface structure of ZNPMs film is the key to their stable separation performance. The chemical cross-linking of amide bonds between microspheres and the coordination of zinc ions increases the stability of the film structure, which also be the basis for the high performance of the film.

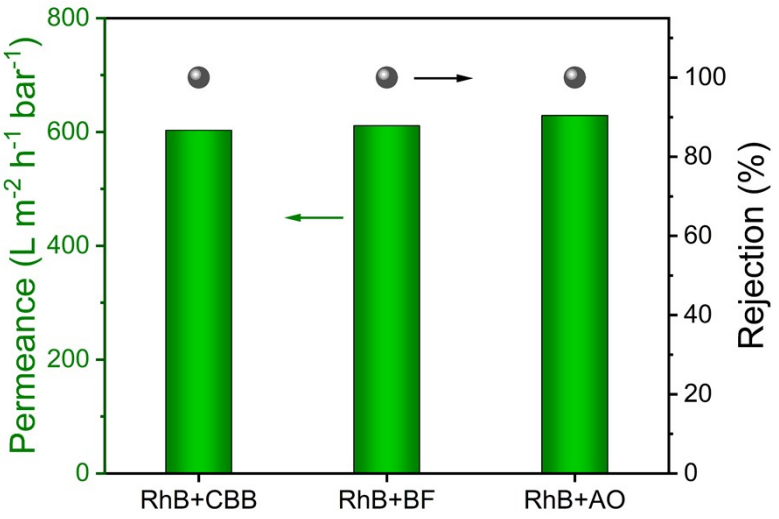

Fig. S17 Separation performance of ZNPMs films for different mixed dyes.

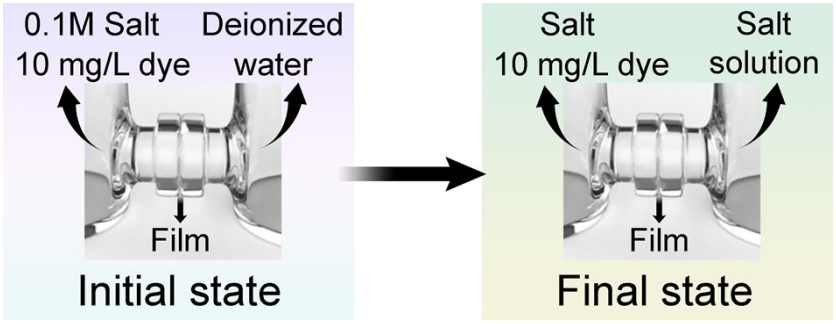

Fig. S18 Schematic diagram of the initial state and final state of the solution on both sides of the H-type electrolytic cell.

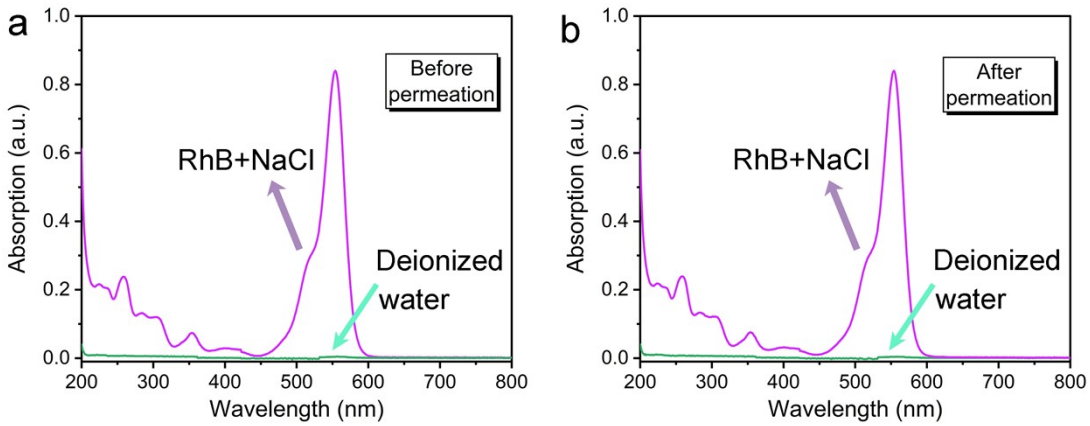

Fig. S19 UV-vis spectra of solutions on both sides of the permeation cell (a) before and (b) after the permeation experiment.

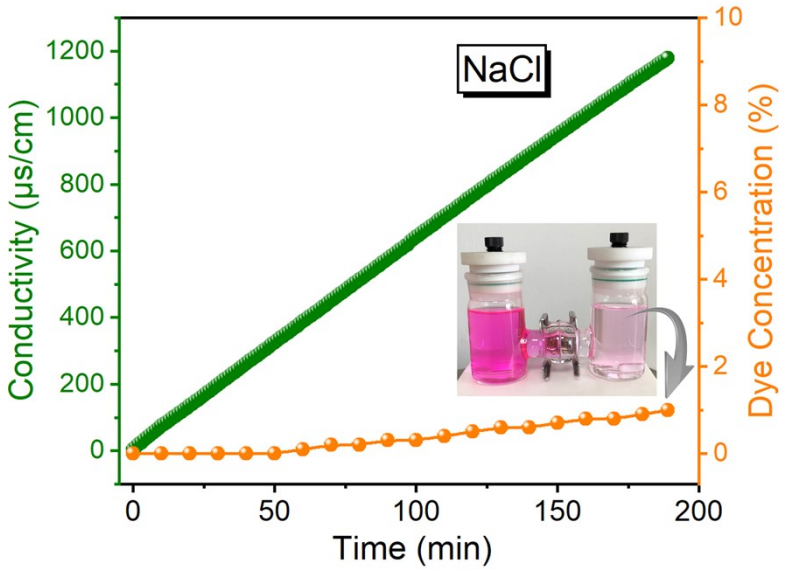

Fig. S20 Permeation pattern of RhB and NaCl in the substrate film (inset is an optical photo of solution colour at the end of the permeation experiment).

Table S1. Concentration-driven diffusion rates of salt ions and dyes

Dye	Salt	Flux (mol m^{-2} h^{-1})
RhB	NaCl	0.481
	$CaCl_2$	0.424
	Na_2SO_4	0.830
	RhB	0

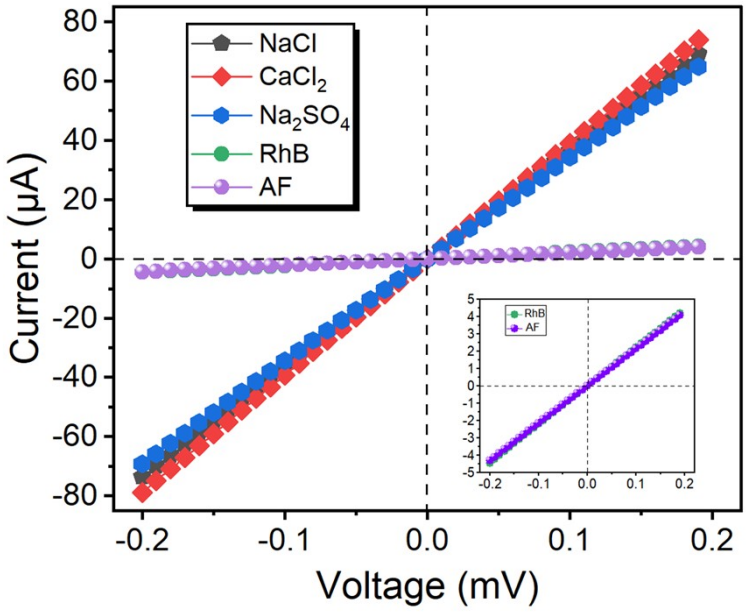

Fig. S21 I−V characteristics of the PVDF substrate films were measured under an electric field in 0.1 M salt (NaCl, $CaCl_2$, Na_2SO_4) solution and 20 mg/L dye (positively charged: RhB, negatively charged: AF) solution.

Theories

Film surface fluid flow model

The permeability and separability of film materials depend on their micro-pore structure (pore size, pore size distribution and pore curvature), the type of fluid, and the interaction between the pore and the fluid. When driven by pressure, the fluid flows from the high-pressure side to the low-pressure side. For some simple gases with linear pressure gradients, the mass transfer process usually follows Darcy's law.[4]

$$J = Q\left(\frac{\Delta_P}{l}\right) = \Pi\Delta p$$

$$J = \frac{F}{V_m A_s}$$

where A_s is the effective pore area, Q is the gas permeation, J is the flow rate, Π is the permeability, F is the volume flow rate, V_m is the molar volume of gas, and l is the film thickness.

Slip length and boundary conditions

In traditional chemical mass transfer calculations, the NS equation is an important method. The NS equation at normal viscosity is shown below:

$$\rho\left(\frac{\partial v}{\partial t} + v \cdot \nabla v\right) = -\nabla p + \eta\nabla^2 v + \rho f_B$$

where f_B is the volume force and η is the fluid viscosity.

Fluid transfilm mass transfer characteristics

In the calculation of fluid transfer across the film, when the thickness of the film is on the micron scale, the mass transfer resistance is mainly determined by the interfacial friction within the pore channel. In contrast, when the film thickness is on the nanometer scale, the mass transfer resistance is mainly determined by the inlet/outlet effect.[5] The relationship between restricted effect resistance and flow rate is as follows Eq.

$$\Delta P_f = \frac{8\eta l Q}{\pi R^4 + 4\pi R^3 L_s}$$

where η is the dynamic viscosity of the fluid, Q is the flow rate, R is the orifice radius, and L_s is the slip length

Diffusion and Computation of Fluids

Diffusion is a fundamental property of molecular transport. Pressure gradients, temperature gradients, concentration gradients, and external fields are the driving forces for the formation of mass transfer diffusion in fluids. In an irreversible process, the molecular flux is proportional to the chemical potential gradient.[6]

$$J = -\frac{Dc}{k_B T}\rho \nabla \mu$$

where $\boldsymbol{J}$ is the molar flux, $\boldsymbol{D_c}$ is the corrected diffusion coefficient, $\boldsymbol{\rho}$ is the average density of the fluid, and $\boldsymbol{T}$ is the temperature.

Interdiffusion occurs when two molecules are mixed. The interdiffusion coefficient can be predicted by Eq.[7]

$$D_{AB} = \frac{3}{16}\frac{\sqrt{4\pi k_B T/M_{AB}}}{n\pi\sigma_{AB}^2\Omega_D} f_D$$

where is the $\boldsymbol{D_{AB}}$ diffusion coefficient, $\boldsymbol{M_A}$ and $\boldsymbol{M_B}$ are the molar masses of substances A and B, respectively, $\boldsymbol{n}$ is the number density of the mixture, $\boldsymbol{\Omega_D}$ is the collision integral, and $\boldsymbol{f_D}$ is the correction term.

Dynamic viscosity coefficient

The properties of the solution mainly include viscosity, osmotic pressure, and diffusion coefficient. Taking sodium chloride as an example, the equation for the diffusion coefficient of the dynamic viscosity coefficient of the solution is as follows:

$$\frac{v}{1000\rho v} = 1 + 0.12C_{NaCl}\exp\left(\frac{C_{NaCl}^{-0.44}}{-3.713T_R + 2.792}\right)$$

$$D = 17.862 \times 10^{-10}\left(\frac{\lambda^+\lambda^-}{\lambda^+ + \lambda^-}\right)(T + 273.15)$$

$$\lambda^+ = 0.00435[1 + 0.0244(T - 18)].$$

$$\lambda^- = 0.00436[1 + 0.0256(T - 18)]$$

where $\boldsymbol{C_{NaCl}}$ is the concentration of the NaCl solution and $\boldsymbol{\lambda}$ is the equivalent conductivity of the ion.

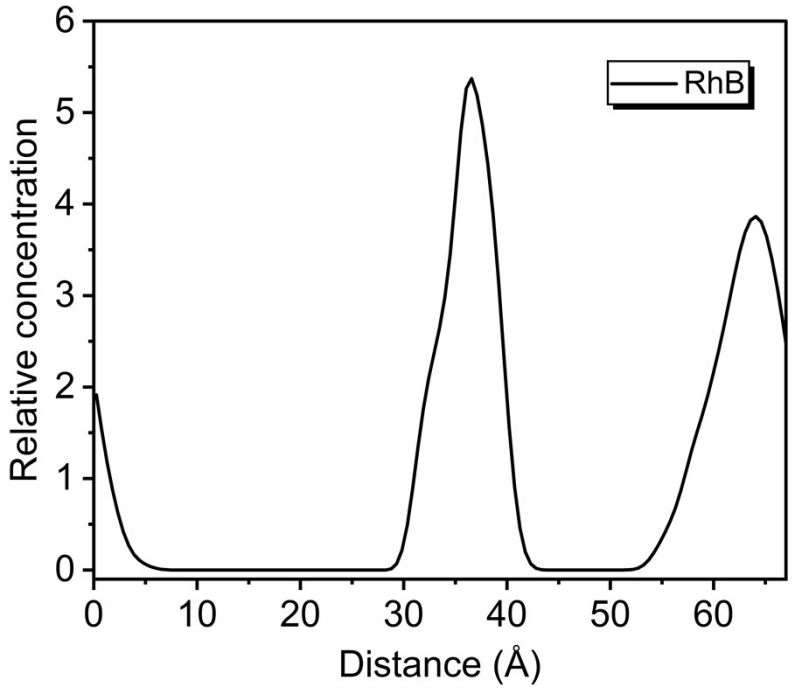

Fig. S22 Relative density distribution of RhB during diffusion along ZNPMs film channels.

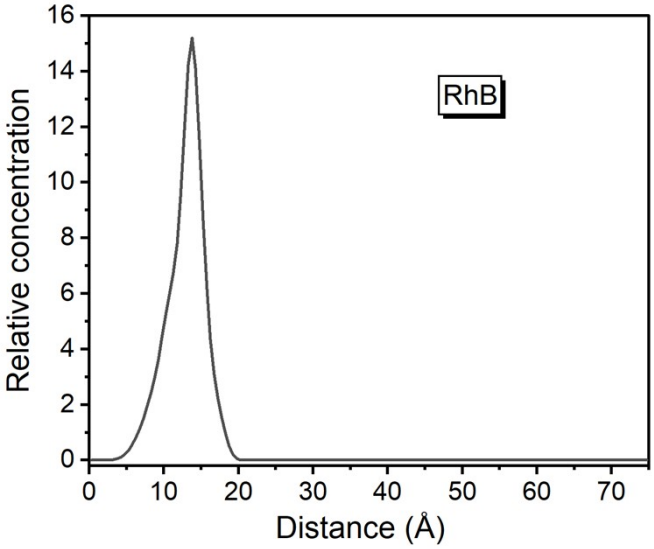

Fig. S23 Relative density distribution of RhB during diffusion along PPy film channels.

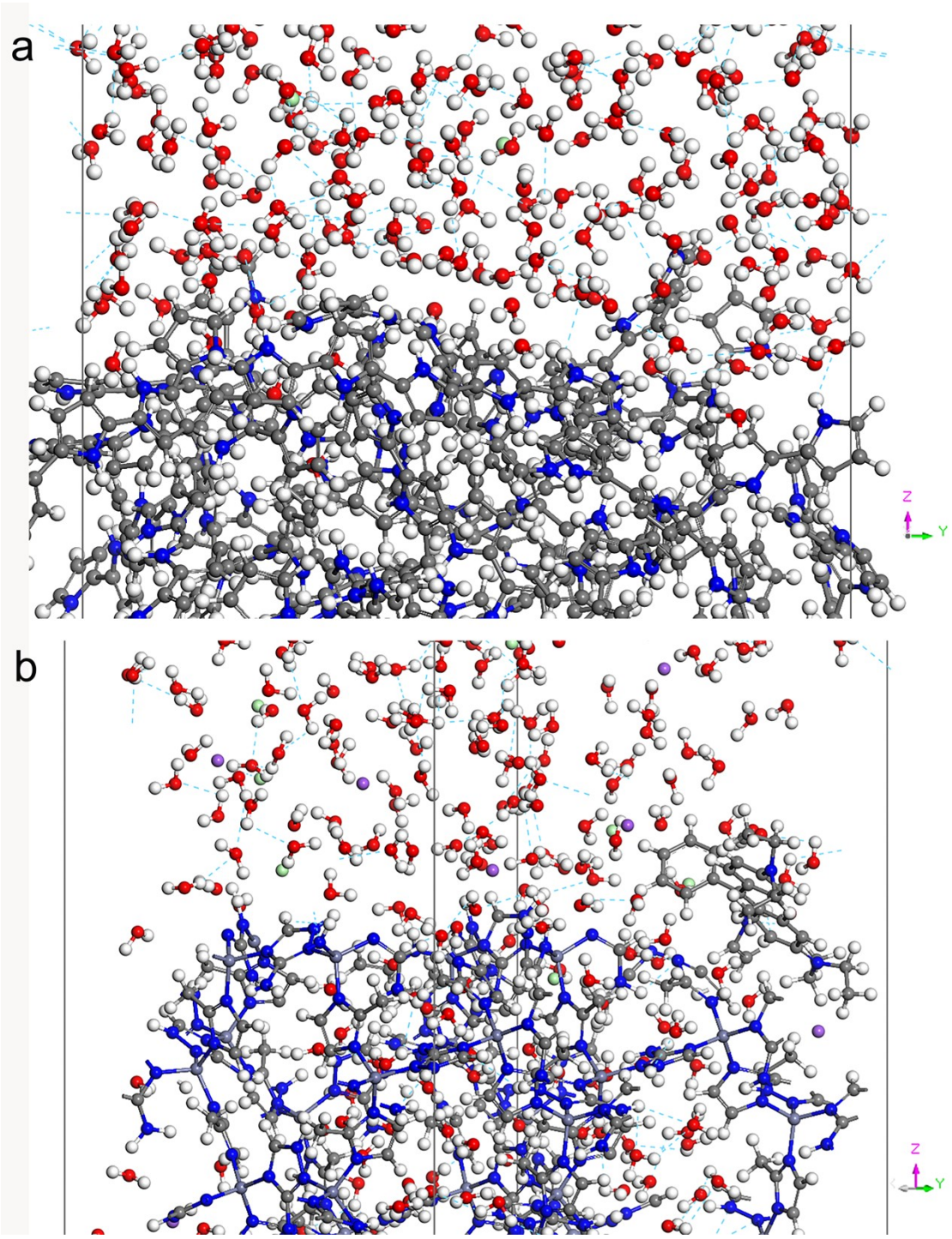

Fig. S24 Distribution of hydrogen bonds in the solution system during diffusion (blue dashed line)

Table S2. Comparison of dye rejection performance of various films

Films	Dye	Initial concentration (mg/L)	Pressure (bar)	Permeance (L m^{-2} h^{-1} bar^{-1})	Rejection (%)	Ref.
Hz-TFPTZ-COF	BB41	50	1	94.69	92	[8]
	MV				88	
CS-MGs/GF	CV	10	0.9	~	99	[9]
	MB				99	
	NR				99	
	RhB				88.1	
MXene/CNT	CBB	20	1	25.8	91.4	[10]
	CR			23.0	92.6	
MXene/COF	MB	10	1	169.3	98	[11]
GO/PAA/CATC	MB	20	0.9	25.6	99.84	[12]
	CR			20.6	99.48	
	RhB			26.7	99.68	
PA/COF–C	CR	100	5	42.0	99.9	[13]
NF-QPEI	LV	100	5	8.21	98.29	[14]
PA-Fe(III)	MB	50	5	190	99.6	[15]
PPSU	AR1	50	2.76	22	93	[16]
Ag/$AgVO_3$-NF	RhB	10	0.98	17.1	85.41	[17]
PAA-MXene/PAN	DR80	100	1	271.26	98.92	[18]
GO/rGO	MB	10	1	23.72	100	[19]
M-S-2	AF	100		74	95.5	[20]
ZNPMs	RhB	10	1	1594	100	This work

BB: basic blue 41; MV: methyl violet; CV: crystal violet; MB: methylene blue; NR: neutral red; RhB: rhodamine b; CBB: coomassie brilliant blue; CR: congo red; LV: leucocrystal violet; AR1: acid red 1; DR80: direct red 80; AF: acid fuchsin

Table S3. Comparison of the performance of various films in dye/salt separation

Films	Pressure (bar)	Permeance (L m^{-2} h^{-1} bar^{-1})	R_{dye} (%)	R_{salt} (%)	Ref.
ZNPMs	0.6	620	RhB: 100	NaCl: 4.3 Na_2SO_4: 3.9 $CaCl_2$: 3.6	This work
PI/SiO_2	3	84.21	CR: 90	Na_2SO_4: 10	[21]
SM/TMC	6	23.5	CR: 99.6 AR 66: 99.0	NaCl: 1.9 Na_2SO_4: 4.5	[22]
LNF	5	114.9	RB 5: 98.8	NaCl: 11.7	[23]
H-PEI/SA	1	57.4	CR: 99.0	NaCl: 12.1	[24]
PET	6	20.4	CR: 99.7	NaCl: 9.3	[25]
PVA-$Cu(OH)_2$	2	37.6	CR: 98.9	NaCl: 13.7	[26]
LNF	2	121.1	CR: 99.4	NaCl: 4.2 Na_2SO_4: 9.8	[27]
CMCS-OA-NaAlg	1	12.6	CBB: 98.5	NaCl: 7.0	[28]
PEA	4	50	CR: 98.8	NaCl: 7.4	[29]
TFC	6	20.6	DR: 99.8	NaCl: 7.0	[30]
POP/TMC	4	31.3	RB5: 99.1	Na_2SO_4: 25.5	[31]
PAN-Tris	1	85	CR: 98.0	NaCl: 5.2	[32]
PSE/PVP(M2)	1	70.7	CR: 98.1	Na_2SO_4: 2.3	[33]
M-MGO	5	44.4	CR: 99.0	NaCl: 3.9	[34]
c-GO/PAN	3	78.5	DR: 99.0	Na_2SO_4: 6.5	[35]
PAN	2	87.5	CR: 99.0	NaCl: 1.5	[36]
TFN	2.5	128.4	CR: 99.9	NaCl: 1.1	[37]
TFC-5	4	20.9	CR: 99.4	NaCl: 23.9	[38]
Su0.6/TMC0.1	6	52.4	CR: 99.4 DR: 98.8	NaCl: 3.3 Na_2SO_4: 11.2	[39]

R_{dye}: dye rejection; R_{salt}: salt rejection; AR 66: acid red 66; RB 5: reactive black 5; DR: direct red 23; RB5: reactive black 5;

References

1. L.-H. Xu, S.-H. Li, H. Mao, Y. Li, A.-S. Zhang, S. Wang, W.-M. Liu, J. Lv, T. Wang, W.-W. Cai, L. Sang, W.-W. Xie, C. Pei, Z.-Z. Li, Y.-N. Feng and Z.-P. Zhao, *Science (New York, N.Y.)*, 2022, **378**, 308-313.
2. S. Li, R. Dong, V.-E. Musteata, J. Kim, N. D. Rangnekar, J. R. Johnson, B. D. Marshall, S. Chisca, J. Xu, S. Hoy, B. A. McCool, S. P. Nunes, Z. Jiang and A. G. Livingston, *Science*, 2022, **377**, 1555-+.
3. S. Wang, Z.-y. Wang, J.-z. Xia and X.-m. Wang, *Journal of Membrane Science*, 2021, **620**.
4. S. Mauran, L. Rigaud and O. Coudevylle, *Transport in Porous Media*, 2001, **43**, 355-376.
5. J. H. Walther, K. Ritos, E. R. Cruz-Chu, C. M. Megaridis and P. Koumoutsakos, *Nano Letters*, 2013, **13**, 1910-1914.
6. B. E. Poling, *The properties of gases and liquids*, The properties of gases and liquids, 1977.
7. O. K. Rice, *Journal of the American Chemical Society*, 1955, **77**, 2031-2032.
8. N. Mokhtari, M. Dinari and H. Fashandi, *Chemical Engineering Journal*, 2022, **446**.
9. Y. Song, J. Pan, M. Chen, Y. Wang, Z. Li and Y. Ge, *Journal of Membrane Science*, 2022, **658**.
10. G. Yi, L. Du, G. Wei, H. Zhang, H. Yu, X. Quan and S. Chen, *Journal of Membrane Science*, 2022, **658**.
11. X. Gong, G. Zhang, H. Dong, H. Wang, J. Nie and G. Ma, *Journal of Membrane Science*, 2022, **657**.
12. W. Tu, Y. Liu, M. Chen, L. Ma, L. Li and B. Yang, *Separation and Purification Technology*, 2022, **296**.
13. L. Chen, C. Zhou, L. Tan, W. Zhou, H. Shen, C. Lu and L. Dong, *Journal of Membrane Science*, 2022, **656**.
14. J. Xiang, H. Li, Y. Hei, G. Tian, L. Zhang, P. Cheng, J. Zhang and N. Tang, *Journal of Water Process Engineering*, 2022, **48**.
15. X. Yang, J. Huang, F. Yang, W. Wang, C. Xue, W. Zhou, Y. Wu, L. Shao and Y. Zhang, *Journal of Membrane Science*, 2022, **653**.
16. Y.-C. Lin, G.-L. Zhuang, P.-F. Tasi and H.-H. Tseng, *Journal of Hazardous Materials*, 2022, **431**.
17. Y. Yue, K. Hou, J. Chen, W. Cheng, Q. Wu, J. Han and J. Jiang, *Acs Applied Materials & Interfaces*, 2022, DOI: 10.1021/acsami.2c04988.
18. Y. Zhang, S. Li, R. Huang, J. He, Y. Sun, Y. Qin and L. Shen, *Journal of Membrane Science*, 2022, **648**.
19. W. Yuan, C. Li, T. Chu, M. Cheng and S. Hou, *Materials Letters*, 2022, **314**.
20. H. Wen, W. Huang and C. Liu, *Desalination*, 2022, **529**.
21. Z. Liu, R. Qiang, L. Lin, X. Deng, X. Yang, K. Zhao, J. Yang, X. Li, W. Ma and M. Xu, *Journal of Membrane Science*, 2022, **658**.
22. Y. Liu, J. Du, H. Wu, C. Cong, H. Zhang, J. Wang and Z. Wang, *Separation and Purification Technology*, 2022, **297**.

23. J. Cheng, Z. Li, X. Bao, R. Zhang, S. Yin, W. Huang, K. Sun and W. Shi, *Journal of Membrane Science*, 2022, **657**.
24. W.-H. Zhang, Z.-J. Liu, M.-J. Yin, Y.-H. Ren, C.-G. Jin, N. Wang and Q.-F. An, *Desalination*, 2022, **535**.
25. M. B. M. Y. Ang, G.-W. Huang, M.-Y. Chu, J. C. Millare, S.-H. Huang and K.-R. Lee, *Journal of Water Process Engineering*, 2022, **48**.
26. Y. Chen, R. Sun, W. Yan, M. Wu, Y. Zhou and C. Gao, *Science of the Total Environment*, 2022, **817**.
27. J. Zheng, R. Zhao, A. A. Uliana, Y. Liu, D. Zhang, X. Zhang, D. Xu, Q. Gao, P. Jin, Y. Liu, A. Volodine, J. Zhu and B. Van der Bruggen, *Chemical Engineering Journal*, 2022, **434**.
28. W. Xie, K. Zhao, L. Xu, N. Gao, H. Zhao, Z. Gong, L. Yu and J. Jiang, *Chinese Chemical Letters*, 2022, **33**, 1951-1955.
29. H. Zhang, F. Xie, Z. Zhao, N. Ul Afsar, F. Sheng, L. Ge, X. Li, X. Zhang and T. Xu, *Acs Applied Materials & Interfaces*, 2022, **14**, 10782-10792.
30. H. Zhou, X. Li, Y. Li, R. Dai and Z. Wang, *Journal of Membrane Science*, 2022, **644**.
31. R. Li, Z. Mai, D. Peng, S. Xu, J. Wang, J. Zhu and Y. Zhang, *Journal of Membrane Science*, 2022, **644**.
32. M. Chen, H. Yang, Z.-l. Xu and C. Cheng, *Journal of Cleaner Production*, 2022, **336**.
33. J.-Y. Zhou, M.-J. Yin, Z.-P. Wang, Y. Shen, N. Wang, Z. Qin and Q.-F. An, *Separation and Purification Technology*, 2022, **283**.
34. Y. Kang, J. Jang, Y. Lee and I. S. Kim, *Desalination*, 2022, **524**.
35. C. Xing, J. Han, X. Pei, Y. Zhang, J. He, R. Huang, S. Li, C. Liu, C. Lai, L. Shen, A. K. Nanjundan and S. Zhang, *Acs Applied Materials & Interfaces*, 2021, **13**, 55328-55337.
36. P. Manna, R. Bernstein and R. Kasher, *Journal of Membrane Science*, 2022, **643**.
37. L. Yang, X. Liu, X. Zhang, T. Chen, Z. Ye and M. S. Rahaman, *Desalination*, 2022, **521**.
38. J. Li, L. Li, Y. Xu, J. Zhu, F. Liu, J. Shen, Z. Wang and J. Lin, *Chemical Engineering Journal*, 2022, **427**.
39. P. Jin, S. Chergaoui, J. Zheng, A. Volodine, X. Zhang, Z. Liu, P. Luis and B. Van der Bruggen, *Journal of Hazardous Materials*, 2022, **421**.